analytical chemistry

pubs.acs.org/ac Article

Locked Nucleic Acid-Enhanced Entropy-Driven Amplifier Combined with Catalytic Hybridization Reaction-Based DNA Circuit for Dual Amplified Detection of Single Nucleotide Polymorphisms and Asymmetric Encryption of Gene Information

Yanlei Li, Zhongfeng Gao,* Yu Du, Yujie Han, Xiang Ren, Dan Wu, Hongmin Ma, Huangxian Ju, Fan Xia, Qin Wei, and Fuan Wang*

Cite This: *Anal. Chem.* 2025, 97, 8506−8515 Read Online

ACCESS | Metrics & More | Article Recommendations | Supporting Information

ABSTRACT: Single-nucleotide polymorphisms (SNPs) play a pivotal role in investigations of disease-associated genes and in the genetic analysis of animal and plant varieties. Therefore, the detection of SNPs is essential for advancing biomedical diagnostics and therapeutics. Here, we report a locked nucleic acid (LNA)-enhanced dual signal amplification strategy for high-contrast detecting single-nucleotide polymorphisms (SNPs) in the KRAS_G12C gene. By integrating entropy-driven amplification with catalytic hybridization reaction, the proposed method achieves significant amplification of fluorescence and resonance Rayleigh scattering signals. The incorporation of LNA modification enhances the thermodynamic stability and reaction kinetics of the DNA computing circuit, resulting in superior sensitivity and specificity for SNPs detection. The method exhibits a low detection limit of 0.19 fM and a wide dynamic range from 1 fM to 0.1 nM for the KRAS_G12C gene. Compared to traditional DNA-based circuits, the LNA-modified system demonstrates enhanced discrimination of single-base mismatches and improved signal gain. Moreover, the proposed method was further demonstrated for its potential application in human serum samples. Impressively, this research not only presents a highly sensitive and selective platform for SNPs detection but also demonstrates its potential for molecular-level information encryption. The incorporation of LNA in dual signal amplification significantly elevates the intricacy and robustness of information encryption. Therefore, this study underscores the potential of DNA-based technologies to serve as a bridge between the era of biomedical research and the emerging Internet of things.

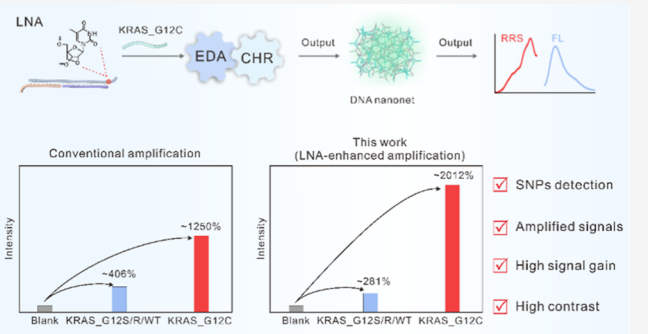

INTRODUCTION

Single-nucleotide polymorphisms (SNPs) are primarily defined as genomic-level DNA sequence variations resulting from alterations in a single nucleotide. These variations can influence the structure and function of encoded proteins and are closely associated with numerous human diseases, including cancers, genetic disorders, and neuropsychiatric conditions.[1−4] Consequently, SNPs have emerged as crucial biomarkers for early disease diagnosis and targeted therapies.[5,6] For instance, mutations in the KRAS gene, which have been identified as significant biomarkers and therapeutic targets, are highly correlated with high-incidence cancers such as pancreatic, colorectal, and lung cancers. Thus, precise and sensitive discrimination of KRAS gene SNPs is crucial for early diagnosis and risk assessment of KRAS-associated cancers.[7−10] However, the identification and quantification of SNPs at the genomic level remain challenging due to difficulties in accurately detecting single nucleotide changes. In recent years, several techniques, including DNA sequencing,[11,12] quantitative real-time reverse transcriptase-polymerase chain reaction (qRT-PCR),[13] time-of-flight mass spectrometry,[14] three-dimensional microchip,[15] and solid-phase microarrays,[16] have been increasingly utilized for SNPs detection. Despite these advancements, traditional methods often face limitations such as costly instrumentation, the need for specialized data analysts, complex procedures, high detection costs, and inadequate specificity and sensitivity, particularly for the detection of specific SNPs site rather than large-scale genotyping analyses.[17] Therefore, the development of an

Received: January 22, 2025
Revised: March 23, 2025
Accepted: April 1, 2025
Published: April 8, 2025

https://doi.org/10.1021/acs.analchem.5c00529
Anal. Chem. 2025, 97, 8506−8515

Scheme 1. Schematic Illustration of the LNA-Enhanced Dual Signal Amplification for Detecting KRAS_G12C Mutant Gene Based on FL and RRS Dual Signals

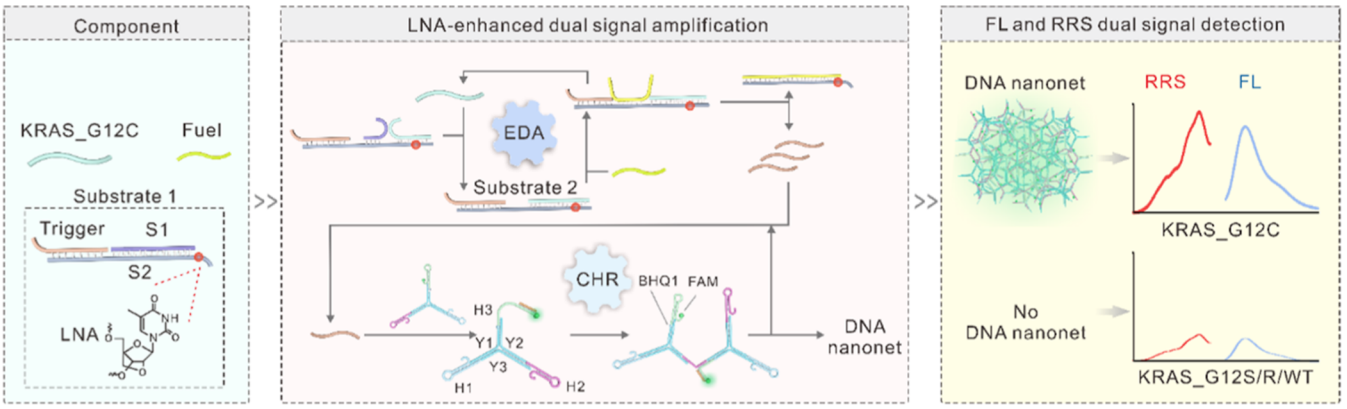

accurate, sensitive, and user-friendly SNPs detection platform continues to present numerous challenges, and there is an urgent need for more effective strategies to meet the practical and diverse application requirements of SNPs detection.

Despite the persistent challenges in SNPs detection, the precise identification of single nucleotides emerges as a paramount consideration in the development of SNPs detection strategies. In previous reports on SNPs biosensors, locked nucleic acid (LNA) has been recognized as an effective tool for distinguishing SNPs.[18−20] LNA is a conformationally restricted ribonucleoside analog that contains a methylene bridge between the 4′-C atom and the 2′-O atom of the ribose ring.[21−23] This constraint on the sugar moiety results in increased affinity and enhanced melting temperature (T_m) values for nucleic acid duplexes.[24] Notably, the T_m reduction of DNA/LNA hybrids containing mismatches is significantly higher than that of DNA/DNA hybrids.[25,26] Thus, the unique structural characteristics of LNA render it an ideal tool for SNPs detection. Although significant progress has been made in the design of LNA-modified probes for SNPs detection, several issues remain unresolved in practical applications, including the optimal positioning of LNA modifications, as well as the unclear thermodynamic and kinetic mechanisms underlying the LNA-enhanced SNPs detection. Therefore, optimizing LNA modifications holds the potential to enhance the sensitivity of SNPs detection.

The low abundance of targets poses another significant challenge for SNPs detection. Typically, single-base mutations occur at a frequency as low as 1% relative to wild-type (WT) alleles, thereby necessitating highly sensitive detection strategies. Generally, enhancing the sensitivity of a detection method often involves integrating signal amplification techniques. Over the past few decades, numerous signal amplification methods have been reported to increase detection sensitivity, such as primer exchange reaction (PER),[27,28] hybridization chain reaction (HCR),[29−31] enzyme cascade catalytic amplification,[32,33] and rolling cycle amplification (RCA).[34−36] The advent of these methods has substantially enhanced the sensitivity of nucleic acid biosensors. In recent years, as signal amplification techniques have matured, dual signal amplification has increasingly replaced single amplification platforms as a new trend for achieving ultrasensitive biosensing. For instance, Exo III-mediated cyclic cleavage combined with RCA was proposed for sensitive detection of microRNA-21 in serum and cell lysates.[37] Catalytic hairpin assembly coupled with PER was established to achieve dual signal amplification, enhancing the sensitivity for protein detection.[38] The dual-CHA-mediated strategy that leveraged CHA to enhance the synergistic amplification effect between DNA walker reaction and HCR, achieving a detection limit down to fg/mL.[39] However, the potential of LNA-enhanced dual signal amplification remains largely unexplored, offering a crucial direction for designing highly sensitive SNPs detection strategies.

Herein, we introduced a highly sensitive and selective LNA-enhanced dual signal amplification for high-contrast genotyping of SNPs in the KRAS_G12C gene. The dual signal amplification incorporated a DNA entropy-driven amplifier (EDA) with a catalytic hybridization reaction (CHR) for producing a highly branched DNA nanonet, amplifying fluorescence (FL) and resonance Rayleigh scattering (RRS) signals. Impressively, the LNA-enhanced dual signal amplification was employed for constructing the DNA computing circuit, which converted the FL and RRS signal values into encrypted ciphertext. The gene sequence of the input KRAS_G12C was securely elucidated through ciphertext decryption. We demonstrated that incorporation of LNA led to enhanced thermodynamic stability and an expanded transducing capacity of the DNA computing circuit by improving the encrypted ciphertext process, thus supporting the elevated security level of information protection. With high robustness and efficiency, this LNA-enhanced dual signal amplification not only represents an advancement in the field of biomedical detection but also holds promise for transforming sensitive information in digital epoch.

EXPERIMENTAL SECTION

Materials and Instruments. All experimental materials, instruments, and processes are detailed in the Supporting Information, with the corresponding oligonucleotide sequences provided in Table S1.

Release the Trigger DNA by EDA Process. The trigger DNA is combined with strands S1 and S2 in equimolar proportions. The mixture is then heated to 95 °C for 5 min, followed by a rapid cooling to 4 °C within 1 min to assemble a ternary complex (substrate 1), which is subsequently preserved in a suitable buffer solution. Following this, 50 μL of the KRAS_G12C buffer is mixed with the preformed substrate 1 at a concentration of 2 μM. The reaction is maintained at 37 °C for 120 min to produce another ternary complex (substrate 2).

https://doi.org/10.1021/acs.analchem.5c00529
Anal. Chem. 2025, 97, 8506−8515

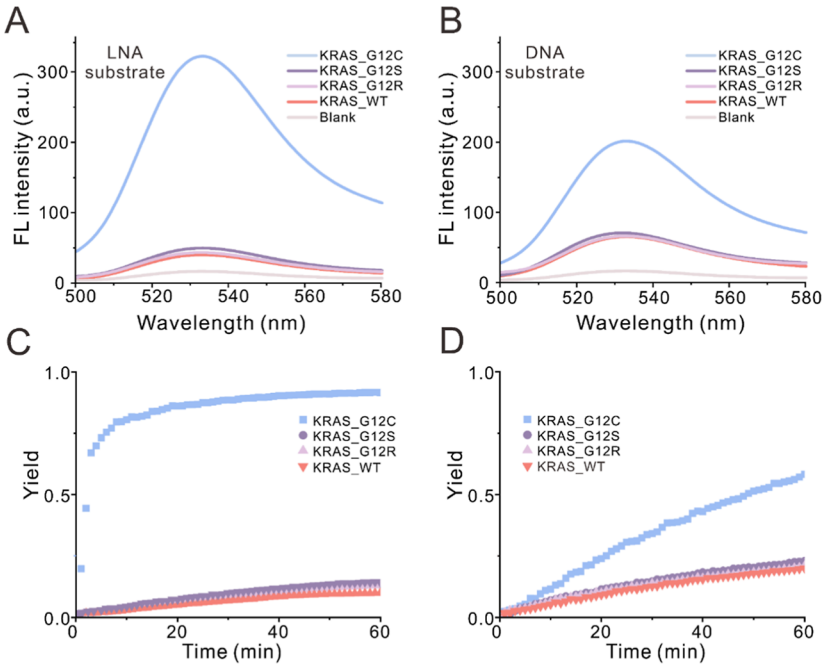

Figure 1. Fluorescence spectra of this system for KRAS_G12C detection using either a substrate containing an (A) LNA nucleotide or (B) a pure-DNA substrate. EDA time: 60 min; CHR time: 60 min. Yield curves for KRAS_G12C detection using the (C) LNA-modified substrate and (D) the pure-DNA substrate. EDA time: 60 min. All KRAS variants (G12C, G12S, G12R, and WT) were prepared at equimolar concentrations (1 nM) in 1 × TE buffer (pH 8.0, 100 mM NaCl, and 5 mM $MgCl_2$).

In the final step, 50 μL of the fuel DNA solution, which is also at a concentration of 2 μM, is combined with the substrate 2 mixture and incubated at 37 °C for an additional 120 min to generate the trigger DNA sequence.

Construction of DNA Nanonet by CHR Process. By mixing Y1, Y2, and Y3 in a stoichiometric balance, then subject the mixture to an incubation period at 90 °C for 3 min. Following this, initiate a controlled cooling process to reach 16 °C, decreasing at a rate of 0.6 °C per minute, and maintain this temperature for 30 min. Concurrently, prepare a mixture of H1, H2, and H3, ensuring the same stoichiometric ratio, and incubate at 90 °C for 3 min. Subsequently, expedite the cooling to achieve 25 °C within a 30 min window, and sustain this temperature for an additional 2 h. Proceed to amalgamate the Y-shaped hybrid DNA strands composed of Y1, Y2, Y3, and H1, H2, H3 in equivalent ratios, and incubate for 1 h to facilitate the assembly of the Y-shaped probe. In the final stage, incubate the Y-shaped probe at a concentration of 200 nM alongside varying concentrations of triggering DNA at 25 °C for 1 h, resulting in the formation of the DNA nanonet structure.

RESULTS AND DISCUSSION

Principle of the LNA-Enhanced Dual Signal Amplification for Detecting KRAS_G12C. In this study, we propose a strategy to construct a highly sensitive and selective LNA-enhanced dual signal amplification that would be useful in the SNPs detection with high contrast. As a proof of concept, we select the KRAS_G12C gene mutation sequence as model target to test the performance and feasibility of the proposed method (for detailed sequence information, see Table S1). As shown in Scheme 1, the EDA substrate that begins the process is composed of a S1 blocker, an LNA-integrated S2, and an initially caged CHR trigger. A conformationally restricted nucleotide analog, LNA, is incorporated into S2 to improve sequence-recognition ability by enhancing the affinity and the T_m of double-stranded DNA (dsDNA). Furthermore, LNA reduces entropic hybridization barriers by restricting conformational flexibility. This effect lowers the activation energy and accelerates binding kinetics through thermodynamic stabilization and enhanced pairing efficiency. At the start of the process, the KRAS_G12C hybridizes with S2, inducing the DNA strand−displacement reaction (SDR) and releasing strand S1 as waste. Fuel DNA triggers the EDA process, where the target is released, allowing it to catalyze a new round of assembly. Simultaneously, the integrated CHR trigger is released to open probe H1, and CHR is initiated by the successive hybridizing of H1, H2 and H3 probes to form a Y-shaped DNA structure. Each assembly process is driven by a SDR with the regenerated CHR trigger, leading to the generation of DNA nanonet by self-assembling of Y-shaped DNA units. After that, we observed an amplified FL signal due to the separation of the fluorophore donor (FAM) from the quenching acceptor (BHQ1). Considering the topology-sensitive feature of RRS on the underlying scaffolds, the DNA nanonet produces a notable RRS signal with high signal gain. As a result, a quantitative assessment of the presence of the KRAS_G12C gene can be acquired from the FL and RRS dual signals.

Feasibility and Characterization of the EDA Cascaded CHR Amplified Reaction. To evaluate whether the incorporation of conformationally restricted LNA nucleotides into strand S2 reduces background noise and enhances signal-to-noise ratios, we systematically compared two substrate designs: (1) LNA-modified sequences inserted at the branch migration-toehold junction and (2) unmodified DNA controls. The results demonstrated that substrates containing either LNA (Figure 1A) or DNA (Figure 1B) can trigger the EDA/CHR iterative reaction. In both cases, the addition of KRAS_G12S, KRAS_G12R, or KRAS_WT sequences led to

https://doi.org/10.1021/acs.analchem.5c00529
Anal. Chem. 2025, 97, 8506−8515

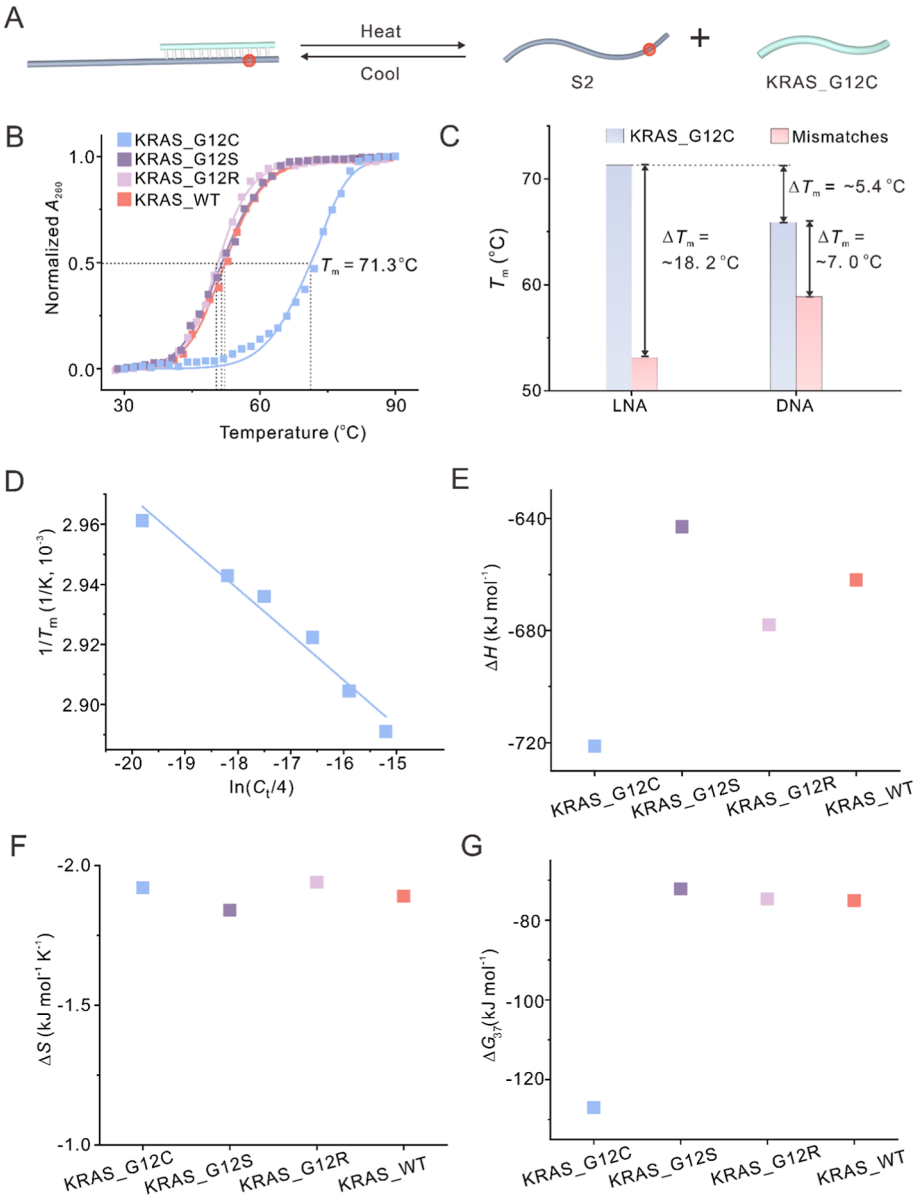

Figure 2. Thermodynamic analyses of SDR stimulated by strands with different sequences. (A) Schematic representation of the thermodynamic binding and melting of DNA double strands. The red dot indicates an LNA base. (B) The melting curves of KRAS_G12C, KRAS_G12S, KRAS_G12R, and KRAS_WT-mediated duplexes using LNA substrate. (C) Comparison of ΔT_m values with the matched target and single mismatched target using LNA-modified and pure DNA substrates. The matched target is KRAS_G12C. The ΔT_m value of a single mismatched target is the average ΔT_m value of KRAS_G12S, KRAS_G12R, and KRAS_WT. The ΔT_m value of KRAS_G12C-induced duplex using LNA and DNA substrates. (D) Thermodynamic analysis of KRAS_G12C interacting with the LNA substrate. Calculated thermodynamic parameters for LNA-mediated SNR: (E) ΔH, (F) ΔS, and (G) ΔG_{37}. All KRAS variants (G12C, G12S, G12R, and WT) were prepared at equimolar concentrations (1 nM) in 1 × TE buffer (pH 8.0, 100 mM NaCl, and 5 mM $MgCl_2$).

low FL intensities and yields, while the addition of the KRAS_G12C sequence led to strong FL intensities and yields for both LNA-modified (Figure 1C) and pure DNA (Figure 1D) substrates. While these findings demonstrated that suggested that KRAS_G12C can initiate the amplification process after toehold binding, chain migration, and trigger assembly, the LNA-modified substrate exhibited superior specificity. In particular, the use of the LNA-modified substrate led to a discriminating factor (DF) of 10.23 (Figure S1), which was 3.04-fold higher compared to the DNA-containing substrate (3.36). Notably, the reaction product, DNA nanonet, possesses large sizes, which might alter the RRS signal. As shown in Figure S2, the RRS intensity induced by the LNA probe was significantly higher than that induced by the DNA probe in the presence of the same KRAS_G12C target, which agrees with the results obtained from FL measurements. In addition, polyacrylamide gel analysis was used to demonstrate the EDA and CHR processes (Figures S3−S5). The DNA nanonet was further confirmed with atomic force microscopy (AFM, Figure S6).

Taken together, these results supported the ability of the proposed strategy to assemble the DNA nanonet and to initiate FL and RRS signals in the presence of the KRAS_G12C. Importantly, we found that the LNA-modified substrate possessed strong single base discrimination ability with high contrast. The improved performance arises from the unique

https://doi.org/10.1021/acs.analchem.5c00529
Anal. Chem. 2025, 97, 8506−8515

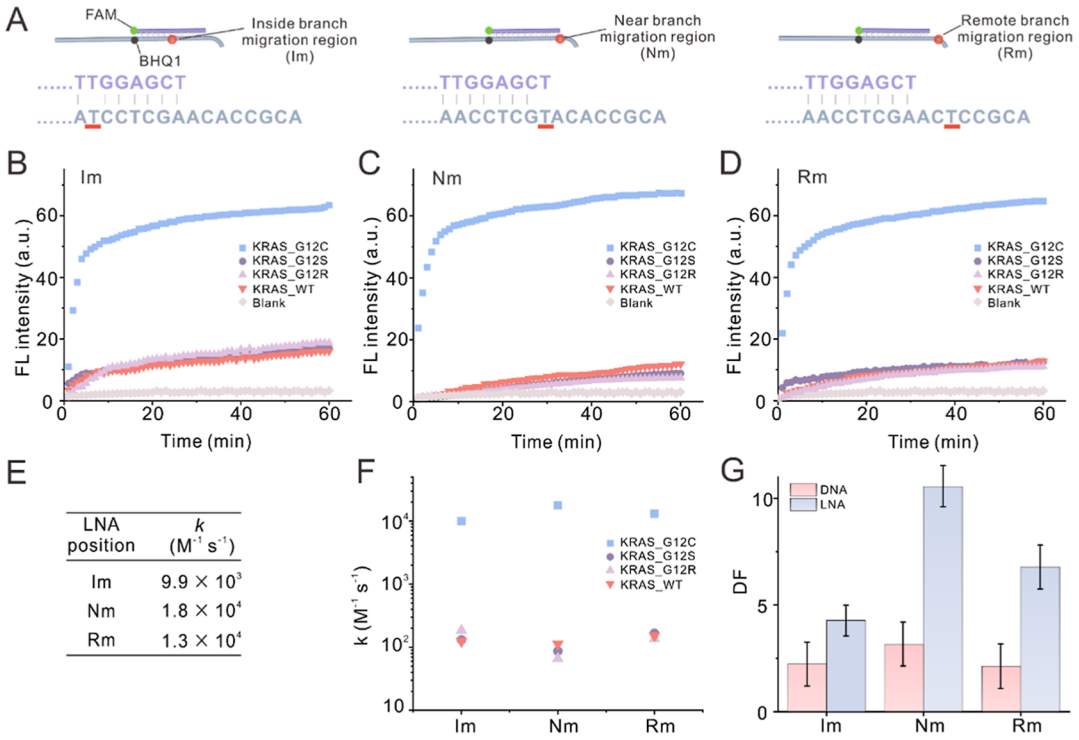

Figure 3. Kinetic analysis of SDR with different modification positions and toehold lengths. (A) Schematic representation of single-base mutations introduced at I_m, N_m, and R_m sites. (B–D) Kinetic curves established upon the addition of Im (B), N_m (C), and R_m (D) substrates to strands with the noted sequences. (E) The calculated rate constants (k) for KRAS_G12C-initiated SDR in the presence of Im, Nm, and Rm substrates. (F) The calculated rate constants for KRAS_G12C, KRAS_G12S, KRAS_G12R and KRAS_WT-initiated SDR in the presence of I_m, N_m, and R_m substrates. (G) DF values for KRAS_G12C detection using LNA-modified and pure-DNA substrates with SNPs at the I_m, N_m, or R_m sites. All KRAS variants (G12C, G12S, G12R, and WT) were prepared at equimolar concentrations (1 nM) in 1 × TE buffer (pH 8.0, 100 mM NaCl, and 5 mM $MgCl_2$).

bicyclic 2′-O,4′-C methylene-bridged structure of LNA, which rigidifies the sugar−phosphate backbone to restrict conformational flexibility.[23,40] This structural constraint reduces entropic hybridization barriers by preorganizing the nucleotide into an A-form helix-like conformation, thereby lowering the activation energy required for base pairing. Simultaneously, the enforced helical geometry positions nucleobases in optimal alignment for Watson−Crick interactions, substantially improving pairing efficiency through enhanced orbital overlap and reduced nonproductive collisions. These dual effects, thermodynamic stabilization via entropy reduction and kinetic acceleration through preorganized hybridization pathways, collectively explain the superior performance of LNA compared to DNA counterparts. Therefore, this system was expected to be useful for highly sensitive SNPs detection.

THERMODYNAMIC PROPERTIES OF THE LNA-ENHANCED SDR

This KRAS_G12C-responsive system leverages LNA's thermodynamic advantages to achieve dual signal amplification, with structural stabilization of key hybridization states enabling robust cascade reaction kinetics through hybridization-directed mechanisms. We first investigated the effect of LNA incorporation on the thermodynamic stability of the dsDNA that the S2 strand forms with the trigger. As shown in Figure 2A, the LNA modification enhanced target recognition, as the LNA/DNA hybrid exhibited a higher T_m value (~71.3 °C, Figure 2B) in comparison to the DNA/DNA hybrid (~65.9 °C, Figure S7A). This increased T_m value of ~5.4 °C with perfectly matched DNA duplex upon integrating a LNA base suggested an enhanced binding affinity. In addition, the dsDNA formed between the LNA-modified substrate and a mismatched target had a significantly lower T_m value (ΔT_m ~18.2 °C) than that formed with the matched target, and the ΔT_m value attained with the LNA-modified substrate was larger than that attained with the pure DNA substrate (~7.0 °C; Figures 2C and S7B–D). The increased ΔT_m value of LNA/DNA hybrids facilitates the identification of SDR in the presence of the KRAS_G12C, thereby enhancing sensitivity and selectivity.

To probe the binding event further, we extracted thermodynamic values from the melting profiles. Specifically, the values of ΔH, ΔS, and ΔG_{37} were determined using previously established methods that assume two-state melting transitions.[41] Data fitting was restricted to the transition region (θ = 0.15–0.85) corresponding to the two-state melting model assumptions. The thermodynamic parameters, ΔH, ΔS, and ΔG_{37}, were determined from graphs of $1/T_m$ versus $\ln C_t/4$ (Figures 2D and S8 and S9). The duplex formed with KRAS_G12C was associated with a much lower ΔH value (Figures 2E and S10) than that formed with mismatched targets, while the entropic contributions were significantly higher (Figure 2F). Accordingly, the KRAS_G12C duplex was associated with a much lower ΔG_{37} (−127 kJ mol^{-1}, Figure 2G) as compared with KRAS_G12S, KRAS_G12R, and KRAS_MT (Table S2). We also determined that the LNA modification reduces the ΔG_{37} by ~17 kJ mol^{-1}, consistent with a high affinity of LNA-DNA base pairs (Figure S11).

To compare the mismatch discrimination of the LNA-modified substrate to that of the pure DNA substrate, the free energy of mismatch discrimination ($\Delta\Delta G_{37}$) was defined as

https://doi.org/10.1021/acs.analchem.5c00529
Anal. Chem. 2025, 97, 8506−8515

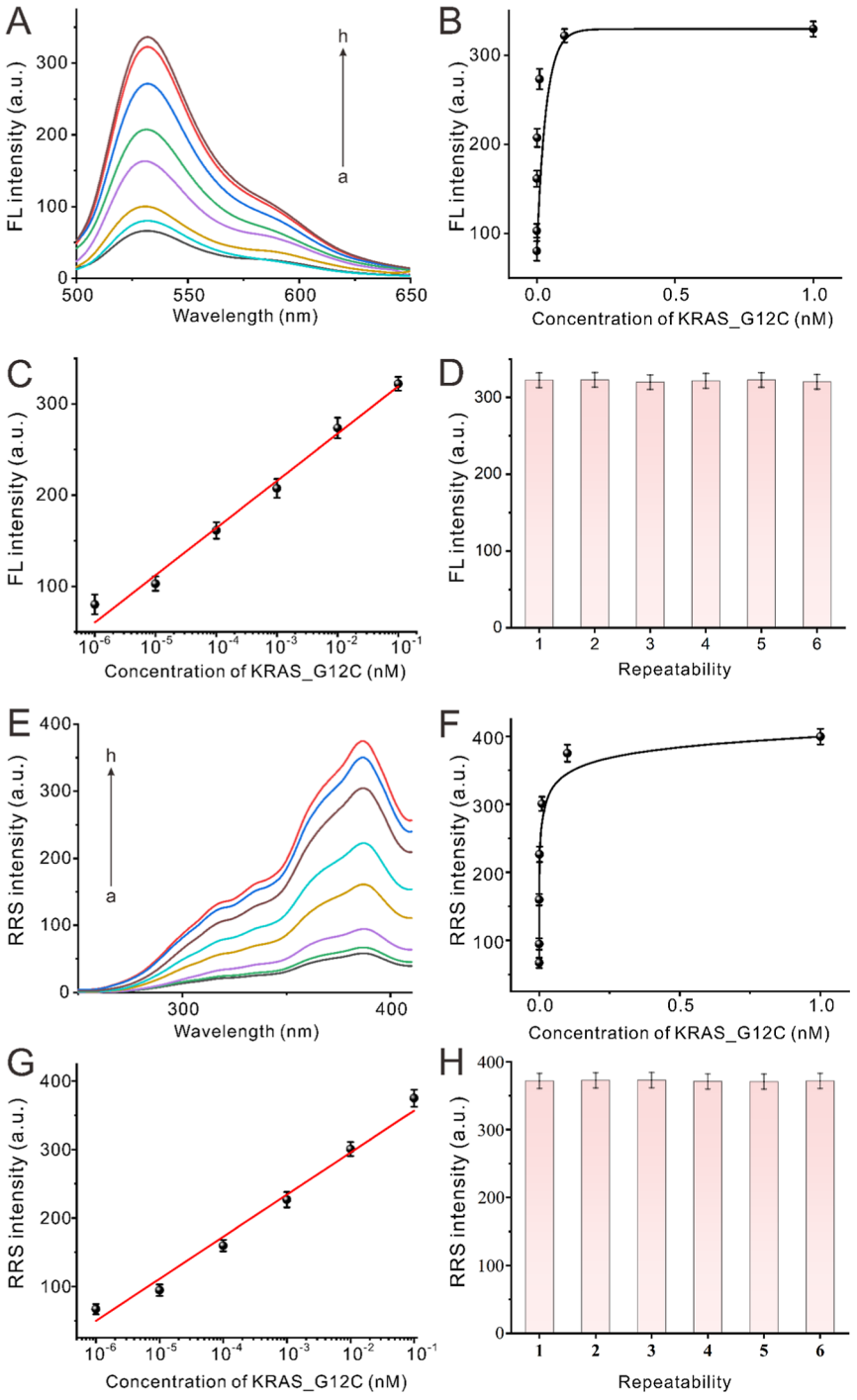

Figure 4. Sensitivity of the proposed DNA computing circuit for KRAS_G12C. (A) FL spectra of different concentrations of KRAS_G12C. From a to h: 0, 1 fM, 10 fM, 0.1 pM, 1 pM, 10 pM, 0.1 nM, and 1 nM. (B) The relationship between KRAS_G12C concentration and FL intensity. (C) Standard curve for KRAS_G12C detection. (D) Stability study of the fluorescent method. (E) RRS spectra of different concentrations of KRAS_G12C. From a to h: 0, 1 fM, 10 fM, 0.1 pM, 1 pM, 10 pM, 0.1 nM, 1 nM. (F) The relationship between KRAS_G12C concentration and RRS intensity. (G) Standard curve for KRAS_G12C detection. (H) Stability study of the RRS method. Error bars: SD of at least three replicates.

the difference between matched and mismatched duplexes ($\Delta\Delta G_{37}$ = ΔG_{37} (mismatch)-ΔG_{37} (match)). Thus, this value quantifies the amount of destabilization due to a mismatch. As shown in Figure S12, the $\Delta\Delta G_{37}$ values associated with the LNA-modified substrate are all larger than those of the pure DNA substrate, indicating that LNA improved both the stability of the duplex and the discrimination of mismatches. Taken together, these results demonstrated that the LNA modification stabilized the binding between the substrate and the matched target, and it also enhanced the mismatch discrimination ability of the system.

EFFECTS OF LNA MODIFICATION POSITION ON SNPS DETECTION

We considered that the position of the LNA might influence the SDR reaction and thus impact the SNPs detection. Therefore, we investigated various substrate strands with the

https://doi.org/10.1021/acs.analchem.5c00529
Anal. Chem. 2025, 97, 8506−8515

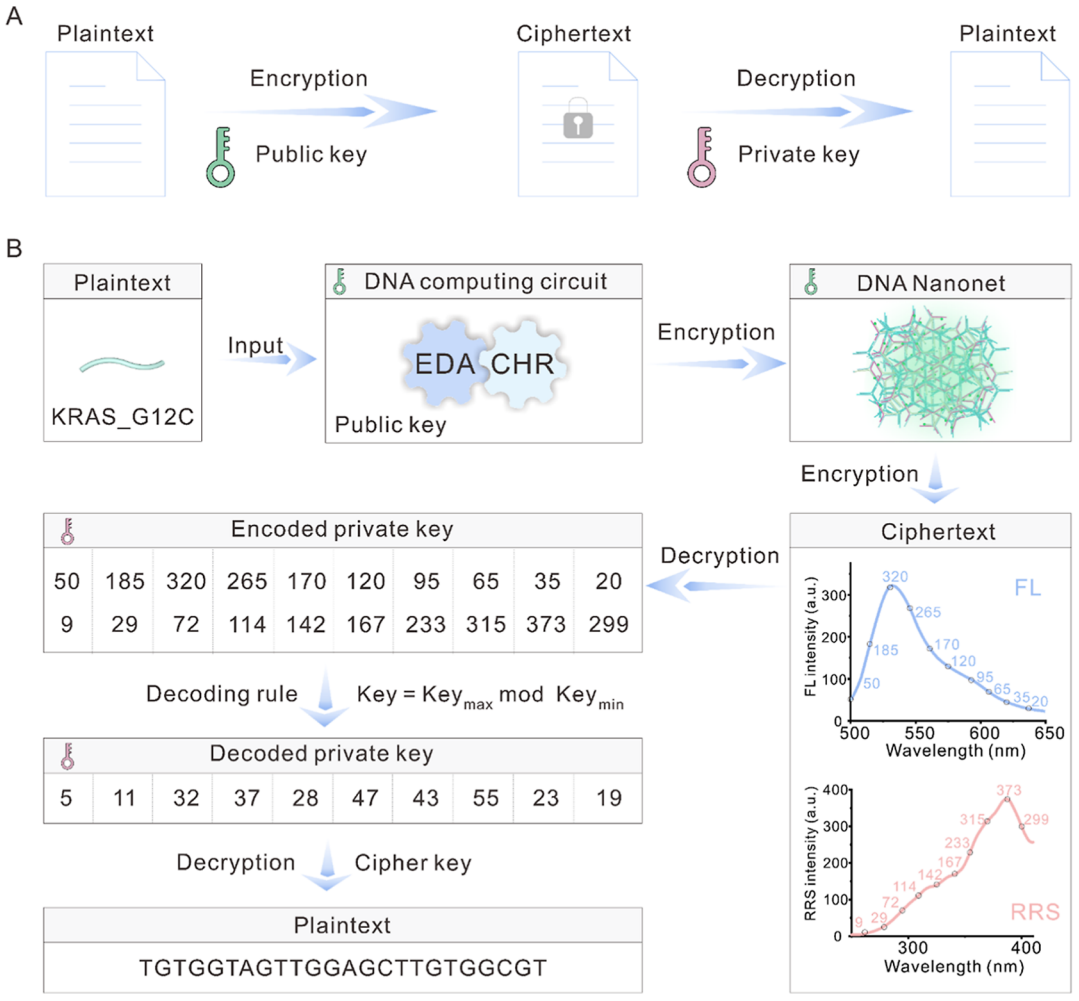

Figure 5. DNA computing circuit for asymmetric encryption. (A) General workflow. (B) Application demonstration of the proposed KRAS_G12C-responsive system for its consequence encryption. The sequence defaults from 5′ end to 3′ end.

single-base mutations within LNA and DNA substrates at three different positions: inside the branch migration region (I_m), near the branch migration region in the toehold (N_m), and remote from branch migration region (R_m) (Figure 3A). The DNA strands were subjected to SDR mediated by a probe labeled with the fluorophore FAM and quenching group BHQ1 (Figure S13). Because formation of the duplex would move the quenching group away from the fluorophore, the progress of the SDR was observed by measuring the donor fluorescence intensity. After 60 min of incubation, regardless of the position of the LNA, the FL intensity significantly increased upon the addition of KRAS_G12C, while the addition of mismatched targets led to only slight increases of FL intensity (Figure 3B–D). We also investigated the kinetics of Im, Nm, and Rm substrates without an LNA base (Figure S14), and the same trend was observed.

The FL intensity was determined to be linearly dependent on the concentration of the fluorescent reporter S1 (Figure S15). Therefore, we converted FL intensity to concentration and then fitted the data obtained from the reporter system to estimate the rate constant (k) associated with the reaction contributing to the observed behavior. It was found that the rate of LNA-mediated SDR was most rapid with the LNA in the Nm position (1.8×10^4 M^{-1} s^{-1}) and slowest with the LNA in the Im position (9.9×10^3 M^{-1} s^{-1}) (Figure 3E). We also determined that relative to KRAS_G12S, KRAS_G12R-, and KRAS_WT-mediated SDR, KRAS_G12C-mediated SDR exhibited higher rate constants with all three of the S2 strands (Figure 3F). Similar conclusions were drawn for pure DNA-mediated SDR (Figure S16).

The DFs were calculated to further investigate the superiority of LNA-mediated SDR for KRAS_G12C detection. As shown in Figure 3G, the maximum DF for the LNA-modified substrate was highest with the Nm version (10.23), and this maximum rate constant was 3.36-fold higher than that observed for the pure DNA substrate. The reason for the higher mutation recognition efficiency of the Nm version relative to the Rm and Im versions might be that the proximal site is situated near where the initial steps of branch migration occur, inducing more pronounced kinetic penalties and more unfavorable thermodynamics upon mismatch.

Sensitivity, Selectivity, and Practicability of the Proposed Method. Following the optimization of detection conditions (Figures S17–S19), we explored the relationship between the FL intensity and the concentration of KRAS_G12C. As depicted in Figure 4A,B, a distinct gradient trend was observed in the FL intensities upon the addition of KRAS_G12C. Linear regression analysis was performed by plotting FL intensity against KRAS_G12C concentration. Within the concentration range of 1 fM–0.1 nM, a linear

https://doi.org/10.1021/acs.analchem.5c00529
Anal. Chem. 2025, 97, 8506–8515

correlation was established between the FL intensity and the logarithm of KRAS_G12C concentration, described by the equation $I = (51.74) \times \log (c_{KRAS\_G12C}) + 370.86$, with a correlation coefficient (R^2) of 0.9903 (Figure 4C). The limit of detection (LOD) was estimated as 0.33 fM (3/slope). Similarly, the RRS signal exhibited a comparable trend for KRAS_G12C detection. As shown in Figure 4E, the RRS signal intensity was dependent on the KRAS_G12C concentration. When plotted against the logarithm of KRAS_G12C concentration, a linear relationship was obtained, with the equation $I = 61.47 \log c_{KRAS\_G12C} + 418.51$ and an R^2 value of 0.9802 (Figure 4F,G). The LOD for this method was determined to be 0.19 fM. Compared to traditional methods, such as colorimetry, photoelectrochemical assays, electrochemiluminescence, and electrochemistry, the dual-signal approach showed superior precision and sensitivity (Table S3).

To assess how feasible the suggested sensing approach was for actual biological samples, recovery tests were carried out using the RRS method and different doses of KRAS_G12C introduced in diluted human serum samples. The results presented in Table S4 revealed that the recoveries ranged from 95.7% to 104%, with RSD values below 5% across all trials. These results confirmed the capability of the developed EDA circuit to detect KRAS_G12C in real samples. The reproducibility of the proposed method was assessed using systems from different batches to measure identical concentrations of KRAS_G12C. The results exhibited highly consistent FL and RRS signals, with low relative standard deviations (RSD) of 3.46% and 4.08%, respectively (Figure 4D,H). These findings demonstrate the high reproducibility of the system.

Asymmetric Encryption of KRAS_G12C Gene Information Using the Proposed DNA Circuit. Innovations in DNA computing circuits have provided new solutions for increasingly important tasks, including information encryption and data security.[42−44] Here, we considered that the proposed KRAS_G12C-detection system could be used to develop a method with improved information security, due to the strong concentration- and time-dependence of the signal output. The resulting asymmetric key model that we developed consists of two parts (Figure 5A), one used for information encryption and another for information decryption. In the first step, a DNA computing circuit with high signal gain is used as a public key for information encryption, and the reaction principle can be made public. However, unless hackers know the corresponding concentration and time used in the encryption process, they will not be able to decrypt the secret message. The second step focuses on decrypting messages using a private key, which is strictly confidential. For example, the KRAS_G12C sequence can be considered plain text that needs to be encrypted. It reacts with an LNA-modified substrate and Y-shaped DNA, and the KRAS-G12C sequence is ultimately encrypted into a DNA nanonet by the DNA computing circuit (Figure 5B).

The DNA circuit's logical verification (Figures S20 and S21) showed precise AND-gate operations (three rounds) with FL/RRS signals achieving logic 1 (no leakage). The KRAS_G12C plaintext was encrypted into FL/RRS ciphertext via DNA nanonet, decrypted using 15 nm-interval patterns. Ten encoded keys ($Key = Key_{max} \bmod Key_{min}$) were decrypted by private cipher keys to retrieve gene sequences (Figure S22). LNA-enhanced circuits increased capacity by 160% (vs DNA-only, Figure S23), enhancing encryption security. Attackers failed due to unknown KRAS_G12C concentrations (preventing FL/RRS replication) and random concentration interference. LNA systems resisted analog attacks (DNA substrates, single-base mismatches; Tables S5−S8), ensuring transmission confidentiality.

CONCLUSIONS

This study presents a LNA-enhanced dual signal amplification strategy that function as a computing circuit for high-contrast genotyping of SNPs in KRAS_G12 and molecular-level information encryption. The LNA-enhanced dual signal amplification integrates EDA with CHR, amplifying the FL and RRS signals. The incorporation of an LNA modification enhances both the thermodynamic stability and the reaction kinetics of the DNA computing circuit. The proposed method has a low detection limit (0.19 fM) and a wide dynamic range (from 1 fM to 0.1 nM) for the KRAS_G12C gene. Compared to a pure DNA computing circuit, this LNA-modified DNA computing circuit offered several intrinsic advantages. First, the enhanced thermodynamic stability of LNA/DNA hybrids significantly improves the discrimination of single-base mismatches, thereby increasing the accuracy and reliability of SNPs detection. Second, the LNA-enhanced dual signal amplification exhibits a higher signal gain, improving the signal-to-noise ratio and thus enhancing the sensitivity and selectivity. Finally, the enhanced ability to discriminate single-base mutations of the DNA computing circuit would prevent unauthorized access by hackers using target analogues, thereby elevating the encryption level in insecure environments. To synergistically balance sensitivity and efficiency, this strategy will undergo future design optimization through two complementary approaches. First, structural modifications such as extend nucleotide toehold-free designs will enhance entropic driving forces by increasing unpaired bases between the target and S2, while precisely positioned LNAs will minimize nonspecific binding. Second, subsequent development will focus on optimizing thermodynamic parameters through ΔG-based hybridization energetics and amplifying reaction kinetics via catalytic acceleration mechanisms employing auxiliary strand displacement facilitators. This research not only introduces a novel approach from biomolecular sensing to biomolecular informatization but also presents valuable opportunities for the development of the DNA-of-Things.

ASSOCIATED CONTENT

Supporting Information

The Supporting Information is available free of charge at https://pubs.acs.org/doi/10.1021/acs.analchem.5c00529.

AFM image, discrimination factors analysis, melting curves, thermodynamic analysis using pure DNA and LNA substrates, calculated thermodynamic values, schematic representation of the KRAS_G12C-induced SDR reaction, kinetic analysis, rate constants analysis, schematic illustration of SDR with various toehold lengths, optimal experiments, Boolean logic tree, truth table, synthetic oligonucleotide sequences, thermodynamic value table, comparison table, the decrypted KRAS_G12C gene information using other inputs (PDF)

https://doi.org/10.1021/acs.analchem.5c00529
Anal. Chem. 2025, 97, 8506−8515

AUTHOR INFORMATION

Corresponding Authors

Zhongfeng Gao − *Key Laboratory of Interfacial Reaction & Sensing Analysis in Universities of Shandong, School of Chemistry and Chemical Engineering, University of Jinan, Jinan 250022, P. R. China;* orcid.org/0000-0002-4667-6212; Email: chm_gaozf@ujn.edu.cn

Fuan Wang − *Department of Gastroenterology, Zhongnan Hospital of Wuhan University, Wuhan University, Wuhan 430072, P. R. China;* orcid.org/0000-0002-3063-2485; Email: fuanwang@whu.edu.cn

Authors

Yanlei Li − *Key Laboratory of Interfacial Reaction & Sensing Analysis in Universities of Shandong, School of Chemistry and Chemical Engineering, University of Jinan, Jinan 250022, P. R. China*

Yu Du − *School of Water Conservancy and Environment, University of Jinan, Jinan 250022, P. R. China;* orcid.org/0000-0002-9002-8845

Yujie Han − *Key Laboratory of Interfacial Reaction & Sensing Analysis in Universities of Shandong, School of Chemistry and Chemical Engineering, University of Jinan, Jinan 250022, P. R. China*

Xiang Ren − *Key Laboratory of Interfacial Reaction & Sensing Analysis in Universities of Shandong, School of Chemistry and Chemical Engineering, University of Jinan, Jinan 250022, P. R. China;* orcid.org/0000-0002-4321-4282

Dan Wu − *Key Laboratory of Interfacial Reaction & Sensing Analysis in Universities of Shandong, School of Chemistry and Chemical Engineering, University of Jinan, Jinan 250022, P. R. China;* orcid.org/0000-0002-8732-5988

Hongmin Ma − *Key Laboratory of Interfacial Reaction & Sensing Analysis in Universities of Shandong, School of Chemistry and Chemical Engineering, University of Jinan, Jinan 250022, P. R. China;* orcid.org/0000-0002-7061-8944

Huangxian Ju − *Key Laboratory of Interfacial Reaction & Sensing Analysis in Universities of Shandong, School of Chemistry and Chemical Engineering, University of Jinan, Jinan 250022, P. R. China; State Key Laboratory of Analytical Chemistry for Life Science, Department of Chemistry, Nanjing University, Nanjing 210023, P. R. China;* orcid.org/0000-0002-6741-5302

Fan Xia − *State Key Laboratory of Biogeology and Environmental Geology, Engineering Research Center of Nano-Geomaterials of the Ministry of Education, Faculty of Materials Science and Chemistry, China University of Geosciences, Wuhan 430074, P. R. China;* orcid.org/0000-0001-7705-4638

Qin Wei − *Key Laboratory of Interfacial Reaction & Sensing Analysis in Universities of Shandong, School of Chemistry and Chemical Engineering, University of Jinan, Jinan 250022, P. R. China; Department of Chemistry, Sungkyunkwan University, Suwon 16419, Republic of Korea;* orcid.org/0000-0002-3034-8046

Complete contact information is available at: https://pubs.acs.org/10.1021/acs.analchem.5c00529

Notes

The authors declare no competing financial interest.

ACKNOWLEDGMENTS

This work was supported by the National Natural Science Foundation of China (22176080, 22090050, and 22274062), National Key Research and Development Program of China (2018YFE0206900), the Natural Science Foundation of Shandong Province (ZR2023YQ015), and the Taishan Scholar Project of Shandong Province (tsqn202312216).

REFERENCES

(1) Chen, D.; Huang, W.; Zhang, Y.; Chen, B.; Tan, J.; Yuan, Q.; Yang, Y. *Angew. Chem.* **2023**, *135*, No. e202304298.
(2) Ortiz, M.; Jauset-Rubio, M.; Trummer, O.; Foessl, I.; Kodr, D.; Acero, J. L.; Botero, M. L.; Biggs, P.; Lenartowicz, D.; Trajanoska, K.; et al. *ACS Cent. Sci.* **2023**, *9* (8), 1591−1602.
(3) Mullard, A. *Nat. Rev. Drug Discovery* **2023**, *22* (3), 167−171.
(4) Yang, X.; Xu, X.; Breuss, M. W.; Antaki, D.; Ball, L. L.; Chung, C.; Shen, J.; Li, C.; George, R. D.; Wang, Y.; et al. *Nat. Biotechnol.* **2023**, *41* (6), 870−877.
(5) Wang, Y.; Cottle, W. T.; Wang, H.; Gavrilov, M.; Zou, R. S.; Pham, M.-T.; Yegnasubramanian, S.; Bailey, S.; Ha, T. *Nat. Commun.* **2022**, *13* (1), 7776.
(6) Guo, K.; Xiao, N.; Liu, Y.; Wang, Z.; Tóth, J.; Gyenis, J.; Thakur, V. K.; Oyane, A.; Shubhra, Q. T. H. *Nano Mater. Sci.* **2022**, *4* (4), 295−321.
(7) Entrialgo-Cadierno, R.; Cueto-Ureña, C.; Welch, C.; Feliu, I.; Macaya, I.; Vera, L.; Morales, X.; Michelina, S. V.; Scaparone, P.; Lopez, I.; et al. *Mol. Cancer* **2023**, *22* (1), 86.
(8) Zhang, Y.; Huang, T.; Lv, W.; Yang, K.; Ouyang, C.; Deng, M.; Yi, R.; Chu, H.; Chen, J. *Front. Bioeng. Biotechnol.* **2023**, *11*, 1201320.
(9) Deng, M.; Ouyang, C.; Yang, K.; Lv, W.; Huang, T.; Li, X.; Zhou, M.; Wu, H.; Xie, M.; Shi, P.; et al. *J. Drug Delivery Sci. Technol.* **2022**, *78*, 103953.
(10) Lv, W.; Yang, K.; Yu, J.; Wu, Y.; Zhang, M.; Liu, Z.; Wang, X.; Zhou, J.; Ma, H.; Yi, R.; et al. *J. Biomater. Appl.* **2023**, *37*, 1813−1822.
(11) Samad Hosseini, S.; Jebelli, A.; Vandghanooni, S.; Jahanban-Esfahlan, A.; Baradaran, B.; Amini, M.; Bidar, N.; de la Guardia, M.; Mokhtarzadeh, A.; Eskandani, M. *Chem. Eng. J.* **2022**, *441*, 135988.
(12) Mir, K. U.; Southern, E. M. *Nat. Biotechnol.* **1999**, *17* (8), 788−792.
(13) Khodakov, D.; Li, J.; Zhang, J. X.; Zhang, D. Y. *Nat. Biomed. Eng.* **2021**, *5* (7), 702−712.
(14) Mauger, F.; Jaunay, O.; Chamblain, V.; Reichert, F.; Bauer, K.; Gut, I. G.; Gelfand, D. H. *Nucleic Acids Res.* **2006**, *34* (3), No. e18.
(15) Wang, Y. K.; Wang, M.; Cheng, S. B.; Chen, Y. J.; Li, C. W.; Xie, M.; Huang, W. H. *View* **2023**, *4* (1), No. e20220054.
(16) Chang, K.; Deng, S.; Chen, M. *Biosens. Bioelectron.* **2015**, *66*, 297−307.
(17) Zhang, Y.; Wang, C.; Zou, X.; Tian, X.; Hu, J.; Zhang, C.-y. *Nano Lett.* **2021**, *21* (10), 4193−4201.
(18) Gao, Z. F.; Ling, Y.; Lu, L.; Chen, N. Y.; Luo, H. Q.; Li, N. B. *Anal. Chem.* **2014**, *86*, 2543−2548.
(19) Sau, S. P.; Kumar, T. S.; Hrdlicka, P. J. *Org. Biomol. Chem.* **2010**, *8*, 2028−2036.
(20) Liu, Y.; Huang, H.; Zheng, Y.; Wang, C.; Chen, W.; Huang, W.; Lin, L.; Wei, H.; Wang, J.; Lin, M. *J. Pharm. Biomed. Anal.* **2023**, *235*, 115632.
(21) Kamali, M. J.; Salehi, M.; Fatemi, S.; Moradi, F.; Khoshghiafeh, A.; Ahmadifard, M. *Exp. Cell Res.* **2023**, *423* (1), 113442.
(22) Braasch, D. A.; Corey, D. R. *Chem. Biol.* **2001**, *8* (1), 1−7.
(23) Vester, B.; Wengel, J. *Biochemistry* **2004**, *43* (42), 13233−13241.
(24) Campbell, M. A.; Wengel, J. *Chem. Soc. Rev.* **2011**, *40*, 5680−5689.
(25) Natsume, T.; Ishikawa, Y.; Dedachi, K.; Tsukamoto, T.; Kurita, N. *Chem. Phys. Lett.* **2007**, *446*, 151−158.
(26) You, Y.; Moreira, B. G.; Behlke, M. A.; Owczarzy, R. *Nucleic Acids Res.* **2006**, *34* (8), No. e60.

(27) Saka, S. K.; Wang, Y.; Kishi, J. Y.; Zhu, A.; Zeng, Y.; Xie, W.; Kirli, K.; Yapp, C.; Cicconet, M.; Beliveau, B. J.; et al. *Nat. Biotechnol.* **2019**, *37* (9), 1080−1090.
(28) An, Y.; Kan, A.; Ouyang, A.; Zhang, N.; Jiang, W. *Sensors Actuators B: Chem.* **2023**, *393*, 134284.
(29) Ming, Y.; Liu, Y.; Li, D.; Jiang, B.; Xiang, Y.; Yuan, R. *Bioelectrochemistry* **2025**, *163*, 108888.
(30) Gao, Z.; Qiu, Z.; Lu, M.; Shu, J.; Tang, D. *Biosens. Bioelectron.* **2017**, *89*, 1006−1012.
(31) Huang, L. N.; Zhong, Z. J.; Lu, Q. J.; et al. *J. Anal. Test.* **2022**, *6*, 36−43.
(32) Kou, B.; Chai, Y.; Yuan, Y.; Yuan, R. *Anal. Chem.* **2018**, *90* (18), 10701−10706.
(33) Kröll, S.; Niemeyer, C. M. *Angew. Chem., Int. Ed.* **2024**, *63* (5), No. e202314452.
(34) Zhu, Z.; Yang, L. *TrAC Trends Anal. Chem.* **2024**, *180*, 117902.
(35) Cao, Y.; Ma, C.; Zhu, J. J. *J. Anal. Test.* **2021**, *5*, 95−111.
(36) Shen, X.; Lin, Z.; Jiang, X.; Zhu, X.; Zeng, S.; Cai, S.; Liu, H. *Biosens. Bioelectron.* **2024**, *264*, 116676.
(37) Zhao, W.; Zhang, X.; Tian, R.; Li, H.; Zhong, S.; Yu, R. *Sens. Actuators, B* **2023**, *393*, 134238.
(38) Cao, J.; Song, X.; Chen, Q.; Yuan, R.; Xiang, Y. *Sens. Actuators, B* **2023**, *385*, 133698.
(39) Huang, W.; Zhan, D.; Xie, Y.; Li, X.; Lai, G. *Biosens. Bioelectron.* **2022**, *197*, 113708.
(40) Kaur, H.; Babu, B. R.; Maiti, S. *Chem. Rev.* **2007**, *107*, 4672−4697.
(41) Zheng, L. L.; Li, J. Z.; Wen, M.; Xi, D.; Zhu, Y.; Wei, Q.; Zhang, X.; Ke, G.; Xia, F.; Gao, Z. F. *Sci. Adv.* **2023**, *9*, No. eadf5868.
(42) Li, K.; Chen, H.; Li, D.; Yang, C.; Zhang, H.; Zhu, Z. *ACS Appl. Mater. Interfaces* **2024**, *16*, 68749−68771.
(43) Xie, X.; Wang, S.; Chen, Z.; Yu, Y.; Hu, X.; Ma, N.; Ji, M.; Tian, Y. *ChemBioChem* **2025**, *26*, No. e202400670.
(44) Jiang, C.; Tan, R.; Li, W.; Zhang, Y.; Liu, H. *Small* **2024**, *20* (51), 2406470.

https://doi.org/10.1021/acs.analchem.5c00529
Anal. Chem. 2025, 97, 8506−8515